V25D-0142 - A preliminary study on low-frequency earthquakes at Mt. Fuji, Japan, using the matched filter method

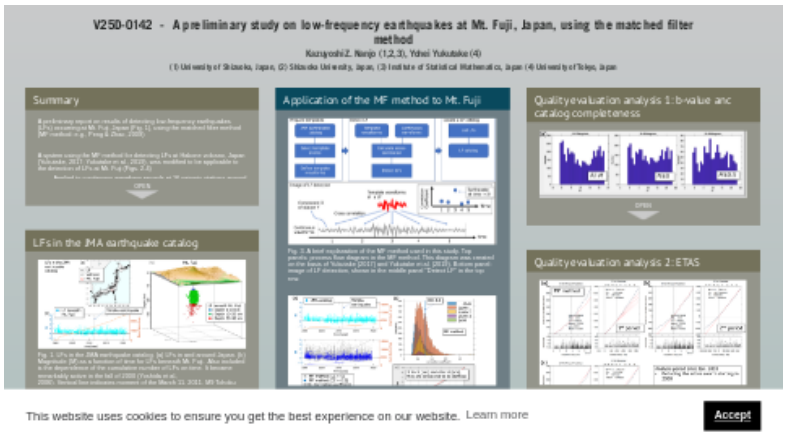

Kazuyoshi Z. Nanjo (1,2,3), Yohei Yukutake (4)

(1) University of Shizuoka, Japan, (2) Shizuoka University, Japan, (3) Institute of Statistical Mathematics, Japan (4) University of Tokyo, Japan

PRESENTED AT:

SUMMARY

A preliminary report on results of detecting low-frequency earthquakes (LFs) occurring at Mt. Fuji, Japan (Fig. 1), using the matched filter method (MF method: e.g., Peng & Zhao, 2009)

A system using the MF method for detecting LFs at Hakone volcano, Japan (Yukutake, 2017; Yukutake et al., 2019), was modified to be applicable to the detection of LFs at Mt. Fuji (Figs. 2-4)

- Applied to continuous waveform records at 16 seismic stations around Mt. Fuji during the period of 2000-2019
- Prepared template waveforms of 27 LFs on the basis of the earthquake catalog maintained by the Japan Meteorological Agency (JMA) (Fig. 1)
- Conducted cross-correlation analysis between the template waveforms and thecontinuous waveform records
- Created a catalog of LFs

3456 LFs occurred in 2000-2019, which is about 1.4 times higher than the number of 2464 LFs listed in the JMA catalog in the same peiod (Fig. 4)

- False detection of LFs seems to be observed (Fig. 4)
- Temporal behavior of LFs in the catalog created in this study, after removing falsely detected LFs from the created catalog, is similar to that in the JMA catalog (Fig. 4)

Quality evaluation analysis was conducted in terms of catalog completeness, the Gutenberg-Richter (GR) law (Gutenberg and Richter, 1944), and the ETAS (Epidemic-type aftershock sequence) model (Ogata, 1985, 1988, 1989)

- Small LFs are likely to be missing from the LF catalog (Fig. 5)
- Larger LFs tend to have fewer numbers and smaller LFs tend to have more numbers (Fig. 5)
- The *b*-value of the GR law is applicable to LFs, a feature found by using the JMA catalog (Fig. 6)
- Applicablility of ETAS to the LF catalog created using the MF method is similar to that to the JMA catalog (Figs. 7 and 8)

Acknowledgements

- The authors thank Y. Noda and T. Kumazawa for help using the MF method and the XETAS program, respectively.
- This study was partially supported by JSPS KAKENHI Grant Number JP 20K05050, the Chubu Electric Power’s research based on selected proposals, the Consortium of Universities & Local Communities in Shizuoka, and the Ministry of Education, Culture, Sports, Science and Technology (MEXT) of Japan, under STAR-E (Seismology TowArd Research innovation with data of Earthquake) Program Grant Number JPJ010217.
- The seismicity analysis software package ZMAP (Wiemer, 2001), used in this study was obtained from http://www.seismo.ethz.ch/en/research-and-teaching/products-software/software/ZMAP.
- The Generic Mapping Tools (Wessel et al., 2013), used for creating some figures are an open-source collection (https://www.generic-mapping-tools.org).
- The XETAS program for making estimates of the ETAS model and for various diagnostic analyses was obtained from http://evrrss.eri.u-tokyo.ac.jp/software/xetas/index.html.
- The JMA earthquake catalog used in this study was obtained from http://www.data.jma.go.jp/svd/eqev/data/bulletin/index_e.html.
- We used the waveform records obtained from the permanent stations of National Research Institute for Earth Science and Disaster Resilience, Earthquake Reseach Institute University of Tokyo, JMA, and Hot Springs Research Institute of Kanagawa Prefectural Government.

LFS IN THE JMA EARTHQUAKE CATALOG

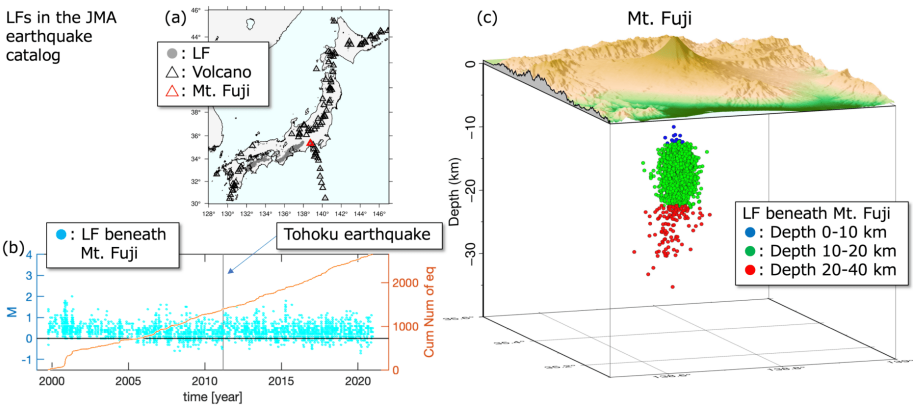

Fig. 1. LFs in the JMA earthquake catalog. (a) LFs in and around Japan. (b) Magnitude (*M*) as a function of time for LFs beneath Mt. Fuji. Also included is the dependence of the cumulative number of LFs on time. It became remarkably active in the fall of 2000 (Yoshida et al., 2006). Vertical line indicates moment of the March 11, 2011, *M*9 Tohoku earthquake. (c) 3D view of LF distribution beneath Mt. Fuji. Majority of LFs is observed in depth 10-25 km (Hamada, 1981; Ukawa et al, 2005).

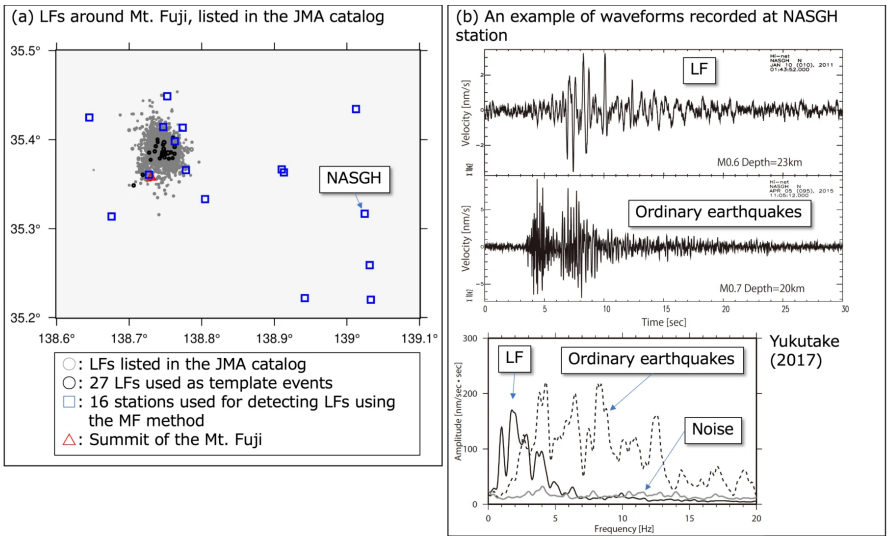

Fig. 2. (a) LFs around Mt. Fuji in the JMA earthquake catalog. (b) Top panel: an example of waveforms recorded for LF and ordinary earthquake (bottom panel) at the NASGH station, indicated in (a). Bottom panel: amplitude spectra of LF and ordinary earthquake, shown in the top panel. Modified from Yukutake (2017).

APPLICATION OF THE MF METHOD TO MT. FUJI

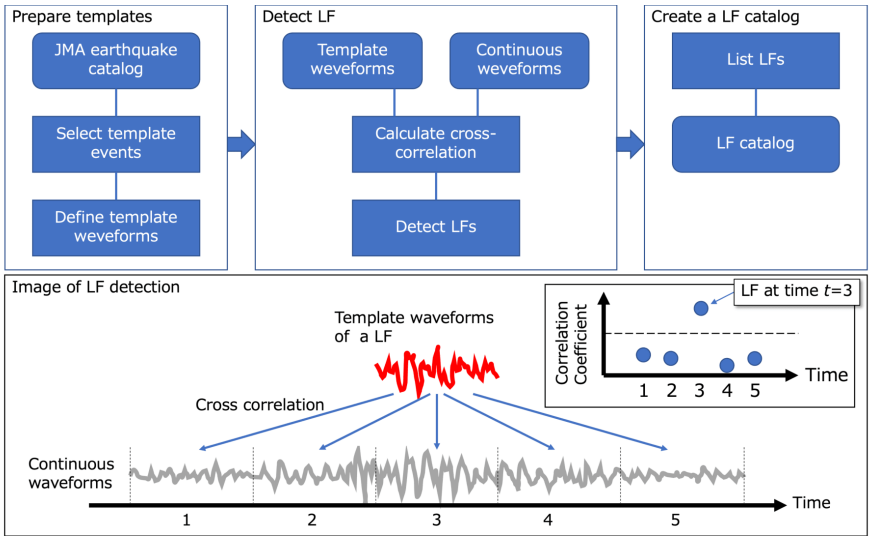

Fig. 3. A brief explanation of the MF method used in this study. Top panels: process flow diagram in the MF method. This diagram was created on the basis of Yukutake (2017) and Yukutake et al. (2019). Bottom panel: image of LF detection, shown in the middle panel "Detect LF" in the top row. Template waveforms and continuous ones are used to calculate cross-correlation coefficient for each of times: t = 1, 2, ..., 5. Inset: If correlation coefficient is larger than a certain threshold level, indicated by dashed line, LF is identified (For this inset, LF is identified at time t = 3). In this study, the threshold level is set to be a value that is 9 times the median absolute deviation.

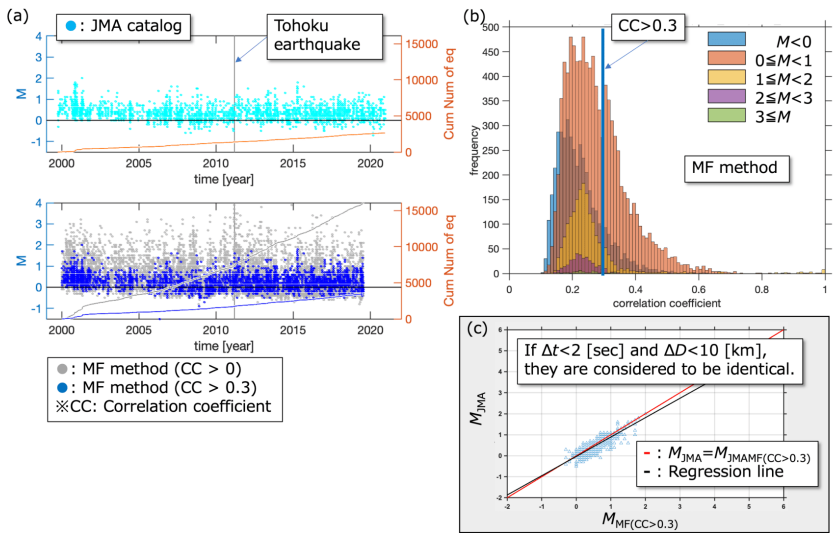

Fig. 4. Initial quality check of LFs detected in this study. (a) Top panel: same as Fig. 1b, except for a larger upper-limit for the right y-axis "Cumulative number of earthquakes". Bottom panel: same as the top panel for LFs. Grey indicates LFs with correlation coefficient (CC) > 0, and blue indicates LFs with CC > 0.3. This value of 0.3 was chosen according to Yukutake et al. (2019), because majority false detection had relatively small correlation coefficients. (b) Histogram of CC for different magnitudes. (c) Comparison in magnitude between LFs in the JMA catalog (M_{JMA}) and LFs with CC > 0.3 ($M_{MF(CC>0.3)}$). LFs in these catalogs are considered to be identical if the hypocentral distance between them (ΔD) is smaller than 10 km and the time difference between them (Δt) is smaller than 2 sec. Red and black lines indicate $M_{JMA} = M_{MF(CC>0.3)}$ and the least-square regression line between M_{JMA} and $M_{MF(CC>0.3)}$, respectively.

QUALITY EVALUATION ANALYSIS 1: B-VALUE AND CATALOG COMPLETENESS

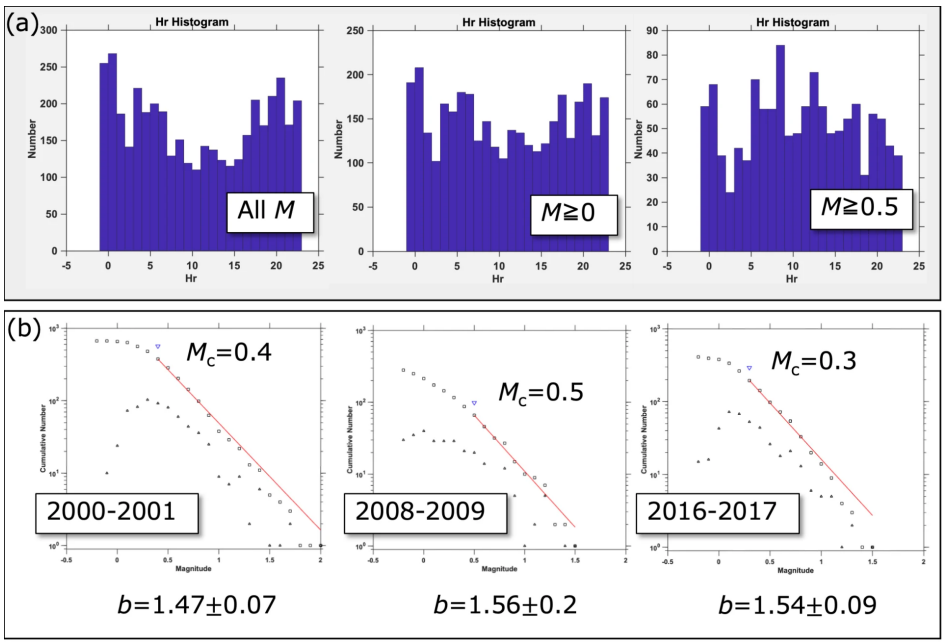

Fig. 5. Catalog completeness and frequency-magnitude distribution of LFs (a) Hour histogram of LFs with CC > 0.3 for different lower cutoff magnitudes: $M \geq$ -1.5 (all magnitudes), $M \geq 0$, and $M \geq 0.5$. (b) Cummulative number (square) and non-cummulative number (upward-pointing triangle) of LFs as a function of magnitude for different two-year periods: 2000-2001, 2008-2009, and 2016-2017. We computed *b*-value of the Gutenberg-Richter (GR) law (Gutenberg and Richter, 1944), given as $\log_{10}N = a - bM$, where *a* and *b* are constants, and *N* is the cumulative number of earthquakes with a magnitude larger than or equal to *M*. To estimate *b*-values consistently over time, we employed the EMR (entire-magnitude range) technique (Woessner and Wiemer, 2005), which also simultaneously calculates the completeness magnitude M_c (downward-pointing triangle), above which all events can be detected by a seismic network. EMR applies the maximum-likelihood method to compute the *b*-value to events with a magnitude above M_c.

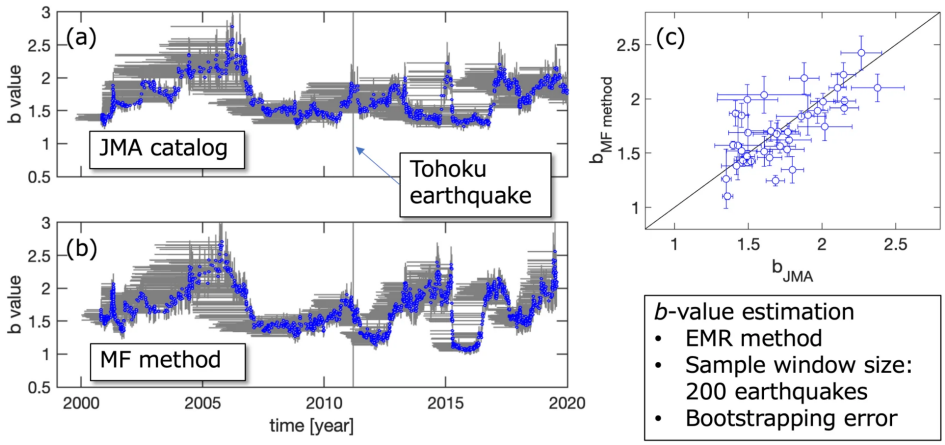

Fig. 6. *b*-value timeseries. (a) Plot of *b*-values as a function of time for LFs beneath Mt. Fuji, listed in the JMA catalog. Uncertainties in *b* (vertical grey segments) were computed by bootstrapping (Schorlemmer et al., 2003). In creating this figure, we used a moving window approach, whereby the window covered 200 events (horizontal grey segment), and plotted *b* at the end of the moving window (horizontal grey segment) that they represent. (b) Same as (a) for LFs in the catalog created in this study. (c) Comparison between *b*-values (b_{JMA}) obtained using data in (a) and those ($b_{\mathrm{MF\ method}}$) obained using data in (b). *b*-values plotted in (a) for time spans of 0.5 years: 2000.0-2000.5, 2000.5-2001.0, ... are used to compute the average and standard deviation of *b* for the corresponding spans. The same computation was done for (b). The average for (b), labeled as $b_{\mathrm{MF\ method}}$ in the vertical axis is plotted by circle against that for (a), labeled as b_{JMA} for each time span. The standard deviations for (a) are used for horizontal error bars and those for (b) are used for vertical error bars. Black line represents $b_{\mathrm{MF\ method}} = b_{\mathrm{JMA}}$.

QUALITY EVALUATION ANALYSIS 2: ETAS

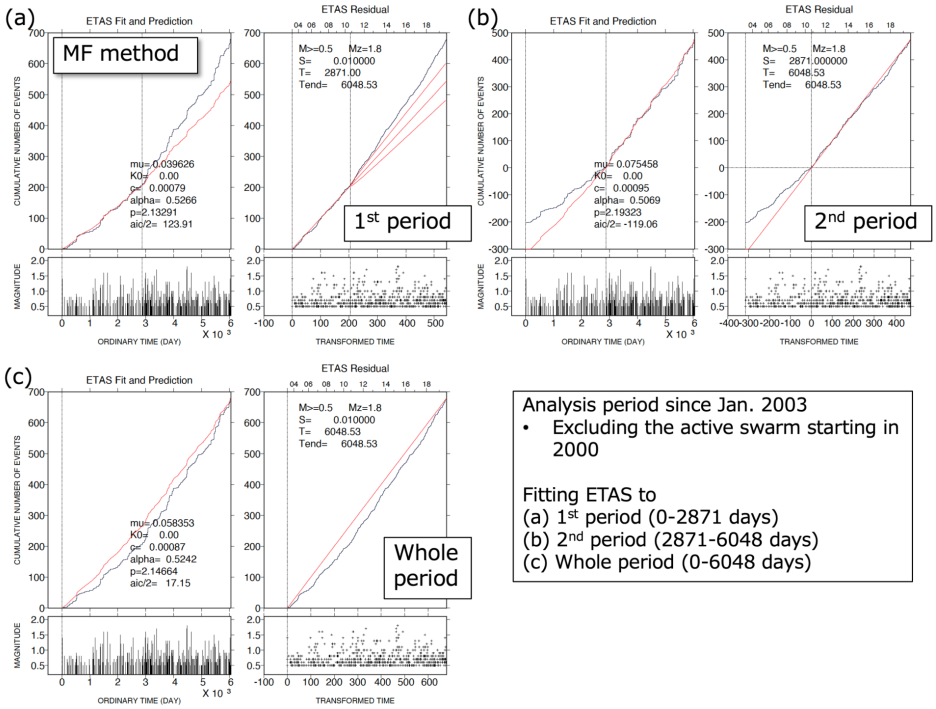

Fig. 7. Fitting of ETAS model to LFs during the time interval from S = Jan. 1, 2003 from T_{end} = July 31, 2019 in the catalog obtained in this study that used the MF method. To conduct the ETAS analysis and visualize model performance, the program package XETAS (Ogata and Tsuruoka, 2016) was used. The emprical cumulative function and magnitudes were plotted versus the ordinary occurrence times (left panels in a, b, and c) and transformed times (right panels in a, b, and c) in the horizontal axis. (a) The theoretical cumulative curves (red) of the fitted ETAS model for the target time interval of 2,871 days since Jan. 1, 2003, the earlier time interval, devided at the elapsed time of 2,871 days (vertical line). This interval is called the 1st period. The parabola for the 95% confidence ranges of the extrapolated curve was added to the right panel. The time of 2,871 days was taken on the basis of change-point analysis concerning seismicity change in Fig. 8. (b) As in (a) except that the target is the later time interval after 2,871 days (the 2nd period). (c) As in (a) except that the target is the entire time interval, called the whole period.

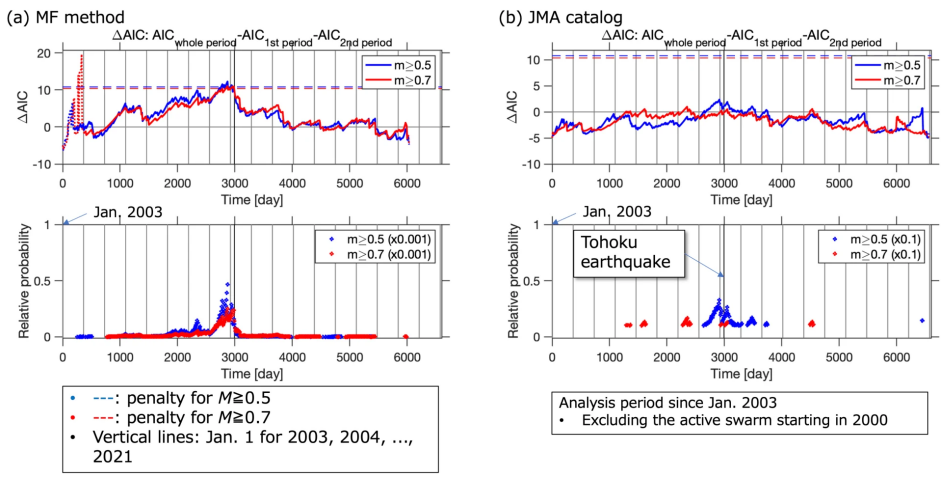

Fig. 8. Change-point analysis, using the ETAS model. Our concern is whether the seismicity changes after some time T_0 in a given period [S, T_{end}] is a problem of model selection (i.e., whether the model fitted separately before and after T_0 then combined together outperforms the model fitted throughout the whole period [S, T_{end}]). On comparing the performances between the models, we consulted the Akaike information criterion (AIC) (Akaike, 1973, 1974, 1977). Our comparison is made between AIC for the combined model and AIC for the model fitted throughout the whole period: $\Delta AIC = AIC_{\text{whole period}} - (AIC_{\text{1st period}} + AIC_{\text{2nd period}})$. $\Delta AIC - 2q > 0$ marks the time T_0 as the significant change point, which means the seismicity patern has significantly changed across the time T_0, where q is the penalty representing the degree of freedom imposed on searching the time T_0 based on the data over the whole period and depend on the total number of LFs (Kumazawa et al., 2010, 2019). (a) Top panel: ΔAIC as a function of time T_0 for LFs in the catalog created by using the MF method. S = Jan. 2003 and T_{end}= July 2019, excluding the active swarm starting in the fall of 2000 (Yoshida et al., 2006). Data that are considered less reliable are indicated by dotted curves. Horizontal dashed lines represent values for $2q$. Bottom panel: relative probability, $\exp(\Delta AIC/2)$, of how likely the model fitted separately before and after T_0 then combined together is superior to the reference ETAS model fitted throughout the whole period, where the probability is computed when $\Delta AIC > 0$. The maximum of ΔAIC is 12.3, above the penalty level. The maximum value is obtained at T_0 = 2,871 days. Model performance at this T_0 is visualized in Fig. 7. (b) Same as (a) for the JMA catalog.